Loss of the Rarefaction Wave during Plasma Sheet Thinning*)

Rudolf TRETLER, Tomo TATSUNO[1)] and Keisuke HOSOKAWA[1)]

Department of Communication Engineering and Informatics, University of Electro-Communications, Tokyo 182-8585, Japan

[1)] *Department of Computer and Network Engineering, University of Electro-Communications, Tokyo 182-8585, Japan*

(Received 29 November 2019 / Accepted 8 June 2020)

A one-dimensional model for plasma sheet thinning [J. K. Chao *et al.*, Planet. Space Sci. **25**, 703 (1977)] according to the Current Disruption (CD) model of auroral breakup is extended to two dimensions. An initial disturbance generates a rarefaction wave. In the 1D model the rarefaction wave propagates tailward at sound velocity, which is regarded as a signature of the thinning. However, in the MHD simulation of the 2D model the rarefaction wave is quickly lost in the plasma sheet recompression, while the thinning continues propagating at a slower velocity. This shows that the dynamics of plasma sheet thinning may be dominated by sheet-lobe interactions that are absent from the 1D model.

Keywords: magnetotail, auroral breakup, current disruption model, two dimensional MHD simulation

DOI: 10.1585/pfr.15.2401053

1. Introduction

The mechanisms behind auroral breakup, a sudden increase of auroral strength during the magnetospheric substorm [1], are not yet entirely understood. While it is known [2] that the three main events in this process are a) magnetotail reconnection, b) cross tail current reduction and c) auroral breakup, their exact order has not been conclusively determined. There are two main competing models, the Near-Earth Neutral Line (NENL) model [3] and the Current Disruption (CD) model.

In the CD model [4], a current disruption instability reduces the cross tail current, breaking the balance of the near-Earth magnetotail plasma, which enters the high-latitude atmosphere and causes the auroral breakup. The magnetotail plasma loss induces a rarefaction wave in the plasma sheet (Fig. 1). The tailward propagation of the rarefaction wave causes a reduction of plasma sheet thickness, eventually leading to magnetotail reconnection.

Chao *et al.* [5] have approximated the initial disturbance that causes the rarefaction wave with an imaginary piston on the near-Earth side of the plasma sheet; earthward movement of the piston generates the rarefaction wave. A simplified model of a piston-bounded 1D gas tube was used to approximate the rarefaction wave in the weakly magnetized neutral sheet plasma, and the result was extrapolated to the full plasma sheet. In this paper, we extend the model to a 2D vertical cross-section of the plasma sheet, including the north and south magnetic lobes. This allows us to take into account the influence of the strongly magnetized lobe plasma, as well as any dynamics that result from the interaction between sheet and lobe plasmas.

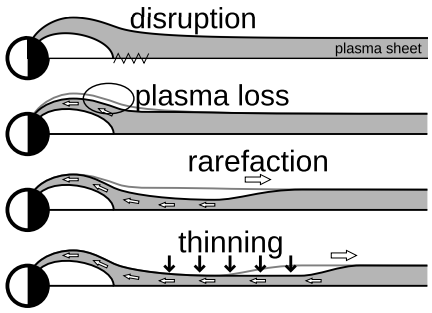

Fig. 1 Stages of the Current Disruption model. (Image adapted from Chao *et al.* [5].)

We show that, although there is a small drop in pressure, the rarefaction wave, which is supposed to be a signature of the CD model, is not noticeable. Furthermore, the propagation velocity of the thinning front shows a strong dependence on lobe conditions.

2. Simulation Setup

2.1 MHD equations

We use the normalized MHD equations in their formulation as a system of conservation laws [6]. System of conservation laws in 2D is

$$\frac{\partial \mathbf{U}}{\partial t} + \frac{\partial}{\partial x} F(\mathbf{U}) + \frac{\partial}{\partial y} G(\mathbf{U}) = 0, \tag{1}$$

where $\mathbf{U}$ is a vector of conserved variables and $F(\mathbf{U})$ and $G(\mathbf{U})$ are respectively fluxes in x and y directions. For the ideal MHD system, the conserved variables are

$$\mathbf{U} = \left(\rho, \rho u, \rho v, \rho w, B_x, B_y, B_z, e\right)^{\mathrm{T}}, \tag{2}$$

author's e-mail: rtretler@protonmail.com

*) This article is based on the presentation at the 28th International Toki Conference on Plasma and Fusion Research (ITC28).

where ρ is the density, $\mathbf{u} = (u, v, w)$ is the velocity vector, $\mathbf{B} = (B_x, B_y, B_z)$ is the magnetic field vector, and e is the total energy. Defining the total pressure $p_{\text{total}} = p + \frac{1}{2}\mathbf{B}\cdot\mathbf{B}$, with plasma kinetic pressure p defined as

$$p = (\gamma - 1)\left(e - \frac{1}{2}\rho\mathbf{u}\cdot\mathbf{u} - \frac{1}{2}\mathbf{B}\cdot\mathbf{B}\right), \tag{3}$$

where γ is the ratio of specific heats (taken to be 5/3), the fluxes in (1) are

$$F(\mathbf{U}) = \begin{bmatrix} \rho u \\ \rho uu - B_x B_x + p_{\text{total}} \\ \rho vu - B_x B_y \\ \rho wu - B_x B_z \\ 0 \\ B_y u - B_x v \\ B_z u - B_x w \\ u(e + p_{\text{total}}) - B_x(\mathbf{u}\cdot\mathbf{B}) \end{bmatrix}, \tag{4}$$

and $G(\mathbf{U})$ the same with the x and y axes reversed.

2.2 Plasma sheet model

For the simulation, we take the relatively flat area of the plasma sheet, where the magnetic field lines are approximately parallel (Fig. 2), and look at the x-y cross-section.

In the neutral sheet is a weakly-magnetized, high-density plasma, $\mathbf{U}_{\text{R}}$ (where "R" stands for "Right"; $\mathbf{U}_{\text{L}}$, "Left", is the initial disturbance region and will be described later). This plasma is sandwiched between the magnetic lobes, with strongly-magnetized, antiparallel, low-density plasmas, $\mathbf{U}_{\text{U}}$ (northern lobe, "Up") and $\mathbf{U}_{\text{D}}$ (southern lobe, "Down").

The inner layer of the plasma sheet, $\mathbf{U}_{\text{sheet}} = \mathbf{U}_{\text{R,L}}$, was assumed by Chao to have a profile described by $\mathbf{B}_{\text{sheet}} = \mathbf{B}_\infty \tanh(y)$. However, testing has shown that the results are almost identical if the plasma sheet contains uniform plasma with no magnetic field. Since the latter is more amenable to analysis, we use a uniform plasma sheet as the initial condition for our simulations.

We assume that prior to the disturbance the plasma sheet was in a steady-state configuration, in which case sheet and lobes are separated by tangential discontinuities. The Rankine-Hugoniot jump condition for a tangential discontinuity [7] is $[p_{\text{total}}] = 0$, where $[X]$ denotes the jump in X when crossing the sheet-lobe boundary. With plasma sheet magnetic field $\mathbf{B}_{\text{sheet}} = \mathbf{0}$, and lobe magnetic field pointing in the x direction, $\mathbf{B}_{\text{U,D}} = \mathbf{B}_{\text{lobe}} = (\pm B_x, 0, 0)$, this condition becomes

$$p_{\text{sheet}} = p_{\text{lobe}} + \frac{1}{2}B_{x,\text{lobe}}^2. \tag{5}$$

Defining the plasma beta as $\beta = 2p/B^2$, we take the first parameter to be the *lobe beta* β_{lobe}. For the second parameter, we define the kinetic temperature ratio τ,

$$\tau = \frac{T_{\text{i,sheet}}}{T_{\text{i,lobe}}} = \frac{p_{\text{sheet}}/\rho_{\text{sheet}}}{p_{\text{lobe}}/\rho_{\text{lobe}}}, \tag{6}$$

where the ion temperature T_{i} is defined through $p = n_{\text{i}}k_{\text{B}}T_{\text{i}}$, $\rho = n_{\text{i}}m_{\text{p}}$, where n_{i} is the ion number density, k_{B} is the Boltzmann constant, and m_{p} is the proton mass.

If we normalize the system so that $p_{\text{sheet}} = 1.0$, $\rho_{\text{sheet}} = 1.0$, and the initial thickness of the plasma sheet is $h_{\text{sheet}} = 1.0$ (Table 1), the steady-state initial condition is determined by the above two parameters, plasma beta β_{lobe} and temperature ratio τ. Finally, we also define the sound velocity $c_{\text{s}} = \sqrt{\gamma p/\rho}$ and the Alfvén velocity $c_{\text{A}} = \sqrt{B^2/\rho}$.

For the initial disturbance, the piston model used by Chao is replaced with a simple earthward plasma flow

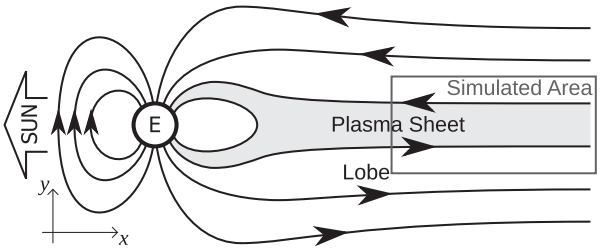

Fig. 2 Rough structure of the Earth's magnetosphere, with the simulated area marked.

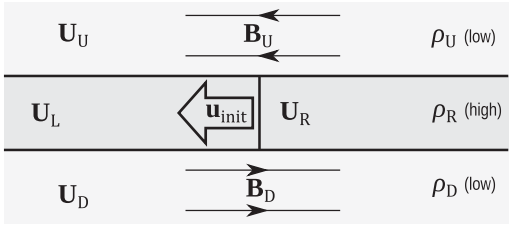

Fig. 3 Initial configuration of the simulated area of the plasma sheet.

Table 1 Units are normalized with respect to the plasma sheet. The first row shows the relationship between physical units and normalized units. The second and third rows show the realistic values for plasma sheet and magnetic lobe, obtained from satellite measurements [7, 8].

	time, t (s)	length, l (km)	velocity, u (km/s)	density, ρ (kg/m^3)	pressure, p (nPa)	mag. field, B (nT)
1.0 normalized units	29.7	1.91×10^5	642	8.35×10^{-22}	0.345	20.8
realistic, sheet	–	–	–	8.35×10^{-22}	0.345	10
realistic, lobe	–	–	–	1.67×10^{-23}	6.9×10^{-4}	30

which will induce the rarefaction wave. The flow is created by assigning an initial velocity $\mathbf{u}_{\rm init} = (u_{\rm init}, 0, 0)$ to the plasma $\mathbf{U}_{\rm L}$ on the Earth side of the plasma sheet (Fig. 3). The $u_{\rm init}$ parameter, which indicates the strength of the disturbance, becomes the third and final parameter of the plasma sheet system.

2.3 Numerical scheme

Since the problem contains discontinuities and will likely develop shocks, we need a robust scheme able to handle them. Here we use the second-order ENO (Essentially Non-Oscillatory) scheme with Lax-Friedrichs flux splitting [9, 10], which has shown a good balance between accuracy, computation speed, and complexity of implementation in preliminary testing.

As the $\nabla \cdot \mathbf{B} = 0$ condition is not explicitly enforced in the MHD equations, the computation is likely to introduce an error and the divergence becomes non-zero. This error accumulates exponentially [11]. Therefore, after every time step we conduct divergence cleaning by solving the Poisson equation $\nabla^2\phi + \nabla \cdot \mathbf{B} = 0$ with the SOR (Successive Over-Relaxation) method, and calculating the corrected magnetic field [6] with $\mathbf{B}_{\rm corrected} = \mathbf{B} + \nabla\phi$.

Finally, for time stepping we use the optimal third-order TVD (Total Variation Diminishing) Runge-Kutta method [12] with a variable time step Δt, calculated so that the CFL number is lower than 0.1.

For the results presented here, the simulation box length was $L_x = 32.0, L_y = 6.0$ units, with $-16 \le x \le 16$, $-3 \le y \le 3$. Each unit is divided into 16 and 32 grid points for a total of, respectively, $(N_x, N_y) = (512, 96)$ and $(1024, 192)$ grid points. The boundary conditions are Dirichlet at $x = -16.0$ (Earth) and $x = 16.0$ (tail), Neumann at $y = -3.0$ (south) and $y = 3.0$ (north), except for the magnetic field component perpendicular to the boundary, which is calculated from $\nabla \cdot \mathbf{B} = 0$. To reduce numerical artifacts, the discontinuities in the initial conditions have been smeared over two additional grid points.

3. Simulations

In the original 1D model, the disturbance is generated with a piston [5]. In our model, the disturbance is generated with an initial velocity, $u_{\rm init}$; this is equivalent to the piston model with piston velocity $u_{\rm p} = u_{\rm init}/2$. The equivalence of the two models was confirmed with a numerical simulation for initial velocity model, comparing it to the exact solution of the piston model.

We next extend the model to two dimensions, adding the north and south magnetic lobes, described with the τ and $\beta_{\rm lobe}$ parameters introduced earlier. A realistic value of the lobe beta would be on the order of $\beta_{\rm lobe} \lesssim 0.01$ [13]; however, this is difficult to achieve in a simulation due to the extremely low kinetic pressure in such a plasma. Therefore, we limit ourselves to $\beta_{\rm lobe} \ge 0.2$. In this extension, Kelvin-Helmholtz instability may arise due to the velocity difference between sheet and lobe [14]. However, we confirmed that it arises only for the weak magnetic field ($B_{x,\rm lobe} \lesssim 0.5, \beta_{\rm lobe} \gtrsim 7$), and that its effect is limited to the far left of the simulation domain ($x \lesssim -3$). Thus it does not affect the following discussions.

An example simulation result is shown in Fig. 4. At time $t = 0$, the left half of the plasma sheet ($x < 0$, $-0.5 < y < 0.5$) begins moving earthward. The pressure drop that the disturbance leaves behind pulls in the

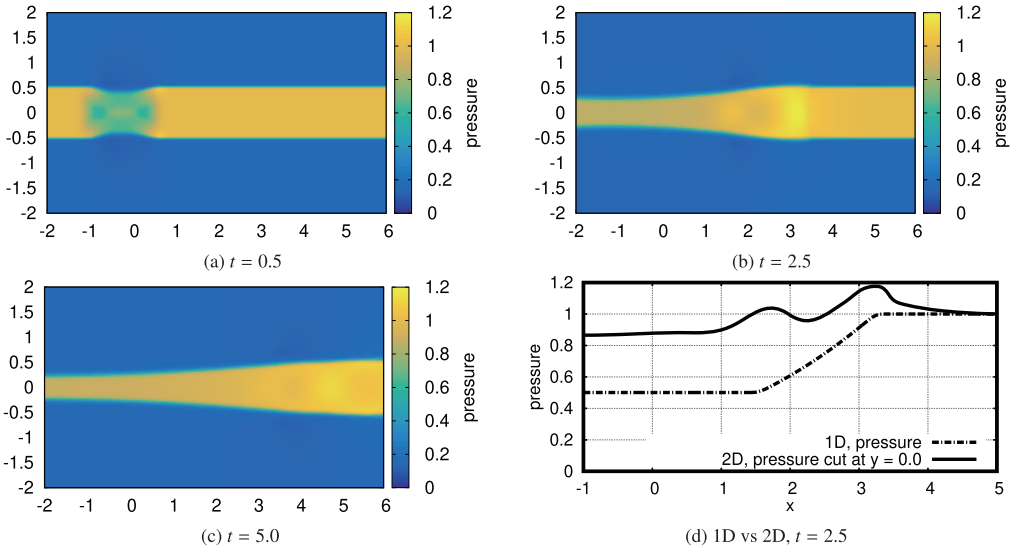

Fig. 4 Example results for a 2D plasma sheet simulation for parameters $\tau = 2.0$, $\beta_{\rm lobe} = 0.2$, $u_{\rm init} = -1.0$. (a), (b), and (c) show the time evolution of pressure. We can observe the initial pressure drop and the beginning of thinning and recompression, followed by propagation of plasma sheet thinning. (d) shows the comparison of pressure at time $t = 2.5$ in 1D and 2D simulation. For 2D, we show the horizontal cut through the center of the plasma sheet, at $y = 0$. Grid density for 1D is 128 points per unit length.

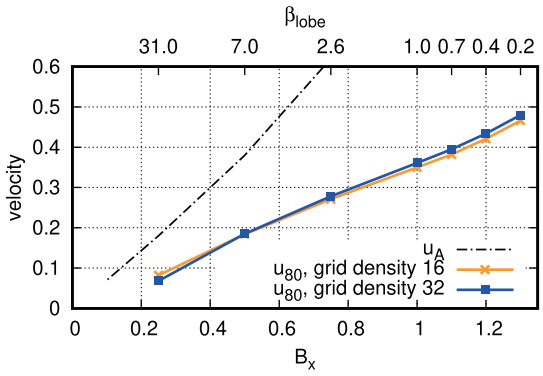

Fig. 5 Dependence of the thinning velocity u_{80} for parameters $\tau = 2, u_{\rm init} = -1.0$ on the lobe magnetic field. Corresponding Alfvén velocity $u_{\rm A}$ is shown for comparison as a dashed line.

surrounding plasma (Fig. 4a). For a few moments, the resulting rarefaction wave is similar to the one in the 1D simulation; however, as the boundary with the magnetic lobes moves inward due to loss of the pressure balance, the plasma sheet is compressed and the rarefaction wave is no longer visible (Fig. 4d). Despite the apparent loss of the rarefaction wave, the earthward plasma flow and the accompanying thinning of the plasma sheet continue (Figs. 4b, 4c).

For further analysis of the plasma sheet thinning, we measure the propagation velocity of its front. Therefore, we need to observe the location of the thinning front through time. To reduce the influence of spurious movement of the boundary, we identify the location where the sheet thickness drops to 80% of the initial condition, and use it for measuring the velocity of the thinning front u_{80}. The results are shown in Fig. 5.

Convergence was checked with several simulations calculated with a different grid size, as well as several simulations with increased L_x and L_y. We can see a good agreement between grid densities 16 and 32, both from pressure profiles as well as in the measured velocity of the thinning front (Fig. 5). More specifically, for $\beta_{\rm lobe} \leq 1.0$, the disagreement in the velocity of the thinning front between 16 and 32 grid densities is below 5%.

4. Comparison of 1D and 2D Model

In the 1D model [5], the initial disturbance generates a rarefaction wave travelling tailward. As the pressure drops behind the wave, the boundary between sheet and lobe is forced to move inward. Since the plasma beta in the sheet is greater than one, the rarefaction wave moves at the sound velocity, $c_{\rm s,sheet}$. The thinning front closely follows the rarefaction wave. The conditions in the magnetic lobes influence only the thinning amount.

In contrast, in the 2D model, the rarefaction wave is lost in the recompression of the plasma sheet (see Fig. 4d); therefore, the pressure drop that should have been what causes the thinning to propagate is absent. However, the thinning continues to propagate nevertheless, indicating that the rarefaction wave is not the sole component of the plasma sheet thinning. Furthermore, the thinning front velocity is lower than the rarefaction wave velocity. This is another indicator that thinning dynamics have separated from the rarefaction wave that initially caused them. Finally, the thinning front velocity shows a strong dependence on the conditions in the magnetic lobes. For example, the thinning front propagates faster when the lobe magnetic field is stronger (see Fig. 5).

5. Conclusion

To summarize, starting from a simple 1D model of the plasma sheet thinning, we have extended it to a 2D configuration by adding the north and south magnetic lobes; this drastically changed the thinning dynamics. We have found that the signature aspect of the Current Disruption model of the plasma breakup—the rarefaction wave—essentially disappears soon after the event begins. However, the plasma sheet thinning keeps propagating, though at a slower velocity which is strongly influenced by the conditions in the magnetic lobes. The dynamics of plasma sheet thinning appear to be dominated by a complicated sheet–lobe interaction that could not be accounted for in the 1D model.

A more in-depth exploration of the parameter space, to determine how the thinning velocity is influenced by the changes in the state of the lobe plasma and the strength of the initial disturbance, will be presented elsewhere.

Acknowledgements

We thank Dr. Takashi Minoshima of the Japan Agency for Marine-Earth Science and Technology (JAMSTEC) for valuable discussions. This research was partially supported by the Rotary Yoneyama Memorial Scholarship.

[1] S.-I. Akasofu, *Polar and Magnetospheric Substorms* (Springer, Dordrecht, 1968) p. 222.
[2] K. Schindler, Space Sci. Rev. **17**, 589 (1975).
[3] D.N. Baker *et al.*, J. Geophys. Res. **101**, 12975 (1996).
[4] A.T.Y. Lui *et al.*, J. Geophys. Res. **82**, 1547 (1977).
[5] J.K. Chao *et al.*, Planet. Space Sci. **25**, 703 (1977).
[6] D. Ryu and T.W. Jones, Astrophys. J. **452**, 785 (1995).
[7] W. Baumjohann and R.A. Treumann, *Basic Space Plasma Physics, Revised Edition* (Imperial College Press, London, 2012) p. 204.
[8] W. Baumjohann *et al.*, J. Geophys. Res. **94**, 6597 (1989).
[9] A. Harten, J. Comp. Phys. **71**, 23103 (1987).
[10] C.-W. Shu, Lect. Notes in Math. **1697**, 325 (1998).
[11] K.G. Powell, ICASE report **94-24** (1994).
[12] S. Gottlieb and C.-W. Shu, Math. Comp. **67**, 73 (1998).
[13] W. Baumjohann *et al.*, Geophys. Res. Lett. **17**, 45 (1990).
[14] S. Chandrasekhar, *Hydrodynamic and Hydromagnetic Stability* (Dover, New York, 1981) p. 507.